



HHS Public Access

Author manuscript

J Am Chem Soc. Author manuscript; available in PMC 2018 September 27.

Published in final edited form as:

J Am Chem Soc. 2017 September 27; 139(38): 13518–13524. doi:10.1021/jacs.7b07311.

The Mechanism of Nitrogenase H₂ Formation by Metal-Hydride Protonation Probed by Mediated Electrocatalysis and H/D Isotope Effects

Nimesh Khadka[†], Ross D. Milton[#], Sudipta Shaw[†], Dmitriy Lukoyanov[¶], Dennis R. Dean[‡], Shelley D. Minter[#], Simone Raugei[^], Brian M. Hoffman^{¶,*}, and Lance C. Seefeldt^{†,*}

[†]Department of Chemistry and Biochemistry, Utah State University, Logan, Utah 84322

[¶]Department of Chemistry, Northwestern University, Evanston, Illinois 60208

[‡]Department of Biochemistry, Virginia Tech, Blacksburg, Virginia 24061

[#]Department of Chemistry, University of Utah, Salt Lake City, UT, 84112

[^]Pacific Northwestern National Laboratory, Richland, Washington 99352

Abstract

Nitrogenase catalyzes the reduction of dinitrogen (N₂) to two ammonia (NH₃) at its active site FeMo-cofactor through a mechanism involving reductive elimination of two [Fe-H-Fe] bridging hydrides to make H₂. A competing reaction is the protonation of the hydride [Fe-H-Fe] to make H₂. The overall nitrogenase rate-limiting step is associated with ATP-driven electron delivery from Fe protein, precluding isotope effect measurements on substrate reduction steps. Here, we use mediated bioelectrocatalysis to drive electron delivery to MoFe protein allowing examination of the mechanism of H₂ formation by the metal-hydride protonation reaction. The ratio of catalytic current in mixtures of H₂O and D₂O, the proton inventory, was found to change linearly with the D₂O/H₂O ratio, revealing that a single H/D is involved in the rate limiting step of H₂ formation. Kinetic models, along with measurements that vary the electron/proton delivery rate and use different substrates, reveal that the rate-limiting step under these conditions is the H₂ formation reaction. Altering the chemical environment around the active site FeMo-cofactor in the MoFe protein either by substituting nearby amino acids or transferring the isolated FeMo-cofactor into a different peptide matrix, changes the net isotope effect, but the proton inventory plot remains linear, consistent with an unchanging rate-limiting step. Density functional theory predicts a transition state for H₂ formation where the S-H⁺ bond breaks and H⁺ attacks the Fe-hydride, and explains the observed H/D isotope effect. This study not only reveals the nitrogenase mechanism

*Corresponding authors: Brian M. Hoffman, Ph. 847-491-3104, bmh@northwestern.edu; Lance Seefeldt, Ph. 435-797-3964, lance.seefeldt@usu.edu.

Supporting Information. The Supporting Information is available free of charge on the ACS Publications website. Experimental procedures, Figures S1–S8, and Animations S1–S2.

ORCID

Lance C. Seefeldt:

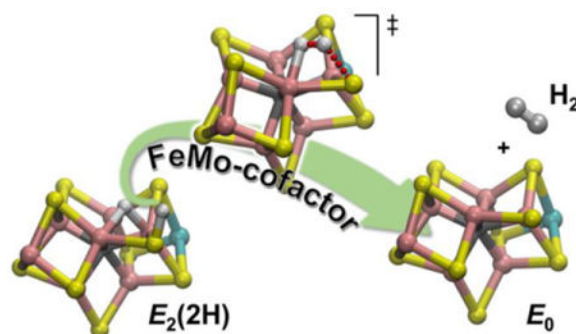
Brian M. Hoffman:

Notes

The authors declare no competing financial interest.

of H₂ formation by hydride protonation, but also illustrates a strategy for mechanistic study that can be applied to other enzymes and to biomimetic complexes.

Graphical abstract



Introduction

Bacterial nitrogenase catalyzes the reduction of dinitrogen (N₂) to two molecules of ammonia (NH₃), making the largest contribution of fixed nitrogen in the global biogeochemical N cycle.¹ The Mo-dependent nitrogenase is comprised of an Fe protein that delivers electrons to the MoFe protein, where the active site FeMo-cofactor (7Fe-9S-1Mo-1C-1R homocitrate) is bound. Recent work has established that the reduction of N₂ at the active site FeMo-cofactor involves reductive elimination (*re*) of two bridging Fe-H-Fe hydrides to form H₂ in a reaction that is linked to N₂ binding and activation to a metal-bound diazene level intermediate (Figure 1).²⁻⁸ The first four electrons and protons are accumulated on the FeMo-cofactor stepwise and are stored as Fe bound hydrides in states designated as E_n where the subscript n indicates the number of electrons/protons delivered.⁹ Nitrogenase is activated for N₂ reduction via *re* of H₂ after the accumulations of four electrons/protons, stored as two [Fe-H-Fe] bridging hydrides and two protons (E₄(4H) state).^{10,11} The *re* mechanism is kinetically and thermodynamically reversible,^{4,7} and the hydrides in the E₄(4H) state are photolytically active.^{5,6} In a parallel, competitive reaction, nitrogenase functions as a 'hydrogenase', producing H₂ through the protonation of a metal-hydride and relaxation to a two-electron less reduced E_{n-2} state (Figure 1B).

The delivery of electrons to the MoFe protein and the active site FeMo-cofactor occurs one electron at a time during the transient association of the Fe protein component of nitrogenase with the MoFe protein component.¹² The Fe protein delivers one electron from its [4Fe-4S] center in a process coupled to the hydrolysis of 2ATP to 2ADP/Pi. The electron is delivered to the MoFe protein active-site FeMo-cofactor, with the P-cluster acting as an electron carrier intermediary.¹³ Earlier work conducted with the artificial electron donor, sodium dithionite, indicated that the dissociation of the oxidized Fe protein with 2 bound ADP was rate-limiting for the overall nitrogenase catalysis.¹⁴ Recent studies using the natural electron donor, flavodoxin, have revealed that the overall rate-limiting step is associated with the release of Pi before the fast dissociation of the oxidized Fe protein with 2ADP from the MoFe protein.¹⁵

As the rate-limiting step for nitrogenase catalysis is associated with electron delivery by the Fe protein, it is not possible to kinetically probe the substrate reduction chemistry at FeMo-cofactor, and in particular measurements of isotope effects on the rates of product formation during enzymatic turnover. Recently, we demonstrated that it is possible to deliver electrons to the MoFe protein without the Fe protein through a mediated electrochemical approach.¹⁶ It was demonstrated that electrons could be delivered to electrode-confined MoFe protein without the Fe protein, and thus without ATP hydrolysis, and that this can drive the reduction of several substrates, as well as the protonation of a metal-hydride to make H₂.¹⁶ This approach thus creates a new rate-limiting step not associated with events in the Fe protein, offering the possibility to probe reactivity of hydrides on FeMo-cofactor using H/D isotope effects. Here, we analyze measured isotope effects on H₂ formation by protonation of metal-hydrides in the MoFe protein using mediated bioelectrocatalysis with a small molecule redox mediator. Coupled with density functional theory calculations, these findings reveal mechanistic insights into this H₂ formation reaction at the nitrogenase active site.

Materials and Methods

Chemicals

All chemicals reagents were purchased from Sigma-Aldrich (St. Louis, MO), unless specified otherwise. Polyvinylamine (95–100%) and ethylene glycol diglycidyl ether (EGDGE, 95–100%) were purchased from PolySciences, Inc. Saturated calomel (SCE) reference and glassy carbon working electrodes were purchased from CH Instruments, Inc.

Bacterial Growth and Protein Purification

Azotobacter vinelandii strains DJ995 (wild-type MoFe protein), DJ1003 (apo-MoFe protein), DJ 1316 (α -70^{Val}→Ala/ α -195^{His}→Gln), and DJ1373 (α -70^{Val}→Ile) were grown and seven histidine-tagged proteins were purified as previously reported. Strain DJ939 (β -98^{Tyr}→His) was also grown and the corresponding non-His tagged MoFe protein was purified as described.¹⁷ nifX protein was purified and complexed with N-methyl formamide (NMF) isolated FeMo-cofactor using a protocol as described previously.¹⁸

Bioelectrocatalysis

All experiments were conducted in an Ar filled glove box. Purified MoFe protein (20 mg mL⁻¹, 15 μ L) was mixed with polyvinylamine (15 μ L at 10 mg mL⁻¹) and EGDGE (2 μ L at 10% v/v); 5 μ L of this mixture was applied to the surface of a planar glassy carbon disk electrode (3 mm diameter) and dried under reduced humidity for 1 hour. Cyclic voltammetry was carried out under an Ar atmosphere in 250 mM HEPES buffer (pH meter reading of 7.2 for H₂O and 6.8 for D₂O) using 667 μ M cobaltocene/cobaltocenium (bis-cyclopentadienyl cobalt (III/II); $E^0 = -1.25$ V vs. SCE) (abbreviated CC) as the electron mediator, Pt as the counter electrode and a saturated calomel electrode (SCE) as the reference electrode. Bis(cyclopentadienyl)cobalt(III) hexafluorophosphate was used to prepare a 6 mM stock in 250 mM HEPES H₂O and 250 mM HEPES D₂O. The pH of both mixtures were adjusted to pH 7.2 and pD 7.2, respectively. The calculated volume was then added from these stocks to 250 mM HEPES H₂O pH 7.2 and 250 mM HEPES D₂O pD 7.2 to achieve the final concentration of 667 μ M cobaltocenium. Solvent deuterium kinetic isotope effect

experiments were undertaken as a function of solvent composition (proton inventory) by mixing solutions containing the buffer made in D₂O or H₂O. The current measured with a mole fraction of D₂O in the mixture (*n*), denoted (*i_n*), was divided by the current in 100 % H₂O (*i_n*/*i₀*), and was plotted against the mole fraction of D₂O (*n*), and the data were well-fitted to the Gross-Butler equation for a one proton transfer reaction,¹⁹

$$\frac{i_n}{i_0} = 1 - \left(1 - \frac{1}{KIE}\right)n = 1 - a n \quad (1)$$

$$a = \frac{KIE - 1}{KIE}$$

The non-catalytic current was determined when bovine serum albumin replaced nitrogenase MoFe-protein. The non-catalytic current was measured at each ratio of H₂O and D₂O. In all cases, the non-catalytic current was very low compared to the catalytic current and did not show any KIE. The non-catalytic current was subtracted from the observed current at each mole fraction to get the net catalytic current that was used for the proton inventory studies.

Quantum Chemical Calculations

A quantum chemical analysis of the effect of the H/D on the formation of H₂ was performed on a simplified model that comprises the FeMo-co and ligands α -275^{Cys}, α -442^{His} (*Azotobacter vinelandii* numbering), and *R*-homocitrate, which were modeled as methylthiolate, imidazole, and dimethyl glycolate, respectively. The quantum problem was solved within the density function theory framework using the gradient-corrected Becke exchange²⁰ and Perdew correlation functionals.²¹ The Ahlrichs VTZ basis set was used for all Fe atoms, the Los Alamos National Laboratory basis set LANL2TZ with an effective core potential was used for the Mo atom, and the 6-311++G** basis set was employed for all atoms coordinated to metal atoms, protic and hydridic hydrogen atoms, and finally the 6-31G* basis set was employed for all of the other atoms. Harmonic nuclear vibrational frequencies were calculated at the optimized geometries using the same level of theory to estimate the zero-point energy and the thermal contributions to the gas-phase free energy, and to evaluate and interpret the experimentally observed isotope effect. The protein environment around FeMo-co was described with a polarizable continuum with a dielectric constant $\epsilon = 4$.²² The adopted model and computational set up was extensively discussed and validated in a previous publication.²³ All calculations were performed with the NWChem quantum chemical code.²⁴

Results and Discussion

Electrochemical Substrate Reduction

As previously established, nitrogenase can catalyze the reduction of several substrates when MoFe protein is immobilized on an electrode surface with cobaltocene/cobaltocenium (CC) as the electron mediator.¹⁶ In the absence of other substrates, MoFe protein only reduces

protons to make H₂. The current observed in the electrocatalysis experiments represents MoFe protein reduction of protons and the background current in the absence of MoFe protein (Figure S1). The background current has been subtracted to yield the net current for H₂ formation (Figure 2).

For catalytic H₂ production by surface-confined MoFe protein in an H₂O/D₂O buffer solution, the measured current, i_n , where n is the fraction of D₂O, is proportional to twice the rate of H₂ release (eqn 2),

$$i_n \propto 2 \frac{dH_2}{dt}(n) \quad (2)$$

As illustrated in Figure 2, which presents cyclic voltammetry (CV) traces for H₂ production by wild-type MoFe protein in solvents ranging from pure H₂O to essentially pure D₂O, the maximum current density ($j = i/A$, where A is the glassy carbon electrode area) is observed at about -1.25 V (vs SCE), shifting slightly in different solvents.

In principle, the H₂ production could be rate-limited by electron/H⁺ delivery to MoFe protein or by H₂ formation itself, or even by an interplay between these processes. To determine the controlling process(es), we monitored the current density for H₂ formation as a function of [CC]. As the [CC] is raised from ~ 50 μ M, the current density first increases, then plateaus at concentrations beyond ~ 500 μ M, indicating saturation for [CC] above 500 μ M, where electron/H⁺ delivery is not rate limiting. In subsequent studies, [CC] ~ 670 μ M was used to ensure that electron transfer (ET) is not rate limiting. This conclusion is confirmed by comparison of the CV for H₂ production with the CV for reduction of NO₂⁻ to NH₃, Figure 3. The roughly 12-fold increase in current for NO₂⁻ reduction not only indicates that ET to MoFe protein during H₂ reduction is not rate-limiting, but also shows that with this CC concentration, electron/proton delivery is at least ten-fold faster than the observed rate of turnover during H₂ formation, thus establishing that electron/proton delivery is not rate limiting under H₂ formation conditions.

Kinetic Isotope Effects on H⁺ Reduction Rates

The kinetic isotope effect on H₂ production was measured by performing cyclic voltammetry with an individual MoFe protein-modified electrode¹⁶ monitored across the full range of H₂O and D₂O buffer mixtures. The advantage of this method is that it eliminates variation in the electrode between experiments at different values of the isotopic ratio, n . As can be seen in Figure 2, the maximum current density in H₂O buffer drops by over 60% in D₂O, corresponding to a kinetic isotope effect (KIE = $j(\text{H}_2\text{O})/j(\text{D}_2\text{O}) = i(\text{H}_2\text{O})/i(\text{D}_2\text{O})$) of greater than 2.5. This KIE is not associated with the reduction/oxidation potential of the CC couple (Figure S1), so these results indicate one or more hydrons (H/D) is involved in one or more of the steps that contribute to the observed rate of H₂ formation. We note that this behavior for electrode-bound MoFe protein is quite different from that during turnover in which electrons are delivered to MoFe protein one-at-a-time from the partner Fe protein. In this case electron delivery is slow and shows no isotope effect (KIE = 1).²⁵

To probe the number of hydrons involved in the rate-limiting step of H₂ production, a proton inventory study was conducted. In this study, the current (i_n) at mole fraction of D₂O, n , divided by the current (i_0) with no D₂O is plotted against the mole fraction (n) of D₂O (Figure 2, inset). The data are fit to the Gross-Butler equation for a single proton transfer step¹⁹ (eq 1) with KIE \approx 2.7. The linear behavior seen is indicative of a single hydron involved in the rate-limiting step.¹⁹ In experiments in which [CC] is lowered \sim 10-fold, slowing the electron delivery, the current is decreased by \sim 1.6-fold in H₂O, and the proton inventory shows distinct ‘upward’ curvature with a decreased KIE, rather than showing the downward curvature expected for a process with multiple hydrons.¹⁹

Kinetic Scheme

The Lowe-Thorneley kinetic scheme for nitrogenase function⁹ in the absence of N₂ incorporates the accumulation of as many as 4[e⁻/H⁺] by FeMo-cofactor, with catalytic formation of H₂ through relaxation of states E_n, $n = 2-4$, as shown in Figure 4, top. In applying this scheme to the bioelectrocatalysis experiments, each step of e⁻/H⁺ delivery is taken as having the same rate constant, k_1 , as seen for electron delivery by the nitrogenase Fe protein, but distinct rate constants are allowed for H₂ release, as in the Lowe-Thorneley kinetic scheme for MoFe protein turnover.⁹ When H₂ formation at E₂(2H) and E₃(3H) is slow compared to electron delivery ($k_2, k_3 \ll k_1$ in the scheme), as is indicated by the experiments presented above, the E₂(2H) and E₃(3H) states once formed would accept an electron before they could evolve H₂, suppressing H₂ evolution from E₂(2H) and E₃(3H) and resulting in H₂ production at E₄(4H) only (as indicated in Figure 4, top). In short, H₂ production involves a two-electron, two-proton ‘reductive activation’ to generate E₂(2H), after which the enzyme then enters a 2-electron, 2-proton steady-state catalytic cycle of H₂ formation that involves E₂(2H), E₃(3H), and E₄(4H). In this cycle, two electrons and two protons are successively delivered to the E₂(2H) state to form first the E₃(3H) and then the E₄(4H) intermediate, each step with rate constant, k_1 . The E₄(4H) state then releases H₂ and regenerates E₂(2H) with rate constant k_4 , which reinitiates the cycle. The steady-state accumulation of E₄(4H) is controlled by the relative values of the rate constants for electron delivery, k_1 , and H₂ release, k_4 .

In steady state, the kinetic model of Figure 4 (top) in fact is precisely equivalent to the truncated cycle between E₀ and E₂(2H) displayed in Figure 4 (bottom), which describes the successive delivery of two electrons and two protons to the E₀ resting state, to form first the E₁(H) and then the E₂(2H) intermediate, each step with rate constant, k_1 . The E₂(2H) state then releases H₂ and regenerates E₀, with a rate constant, k_2 , with the steady state accumulation of E₂(2H) controlled by the relative values of k_1 and k_2 . For simplicity, we henceforth discuss steady-state H₂ formation in terms of the simple scheme of Figure 4 (bottom), with the understanding that it applies equally to the full scheme of Figure 4 (top). We test and confirm this picture below.

To begin the analysis of the electrocatalytic H₂ production by MoFe protein on an electrode according to the truncated kinetic scheme of Figure 4 bottom, and in particular the description of the proton inventory measurements, we start by noting that at steady-state, the measured current, denoted i_p , for a buffer solution where n is the fraction of D₂O is

proportional to the amount of active electrode-bound enzyme, E_0^0 , and the steady-state rate constant, k_n , for the kinetic scheme (eq 3), for which it is readily shown that this rate constant is given by (eq 4),

$$i_n \propto 2 \frac{dH_2}{dt}(n) \stackrel{SS}{\propto} 2k_n \bullet E_0^0 \quad (3)$$

$$k_n \stackrel{SS}{=} \left[\frac{k_1(n)k_2(n)}{k_1(n)+2k_2(n)} \right] \quad (4)$$

Here, k_n , the steady-state rate constant at solvent composition, n , is written as a function of solvent isotope-dependent rate constants for the individual steps of Figure 4 (bottom), $k_i(n)$, $i = 1, 2$, whose form is discussed immediately below, because in principle, either or both the electron transfer (ET)/proton transfer (PT) and H_2 -release steps can show a KIE.

Exchangeable Proton

The linear dependence of i_n/i_0 on n (Figure 2) implies the measured KIE for current/ H_2 production is associated with the activation of a single hydron.¹⁹ We thus begin the analysis by assigning to each of the rate constants k_i for the individual electron/proton transfer and the H_2 -release steps of Figure 4, (bottom) a single-proton, linear proton inventory with an isotope effect of magnitude KIE_i , eq 5,

$$k_i(n) = k_i^o(1 - a_i n); \quad i=1, 2 \quad a_i = \frac{KIE_i - 1}{KIE_i} \quad (5)$$

This is obviously the correct form for electron transfer: proton-coupled electron transfer would exhibit a single-proton inventory with $KIE_1 = 1$; rate-limiting transfer of the electron would yield $KIE_1 = 1$. Although the H_2 formation/release process could in principle involve one or two hydrons in the rate-limiting step, below we show that a 1-proton inventory is appropriate and explain why this is so.

In the standard treatment of the KIE for solution reactions, a proton inventory for an individual kinetic step, such as the form of eq 5, arises because the involved hydron is in 'instantaneous' equilibrium with solvent; in the present case, this means that its exchange with solvent is faster than the kinetic processes of Figure 4. This is quite plausible for the proton bound to sulfur in $E_2(2H)$ or $E_4(4H)$. It would not be so for the bridging hydride/deuteride, which does not exchange with solvent. We first consider the fast-exchange case, then below treat the slow-exchange case.

Proton inventory for the current

We here consider the interplay of electron and proton transfer and H_2 production in controlling the current as manifest in the overall behavior of the proton inventory for H_2

production, and thus for the electrochemical current i_n (eqs 3, 4). Incorporation of eq 5 into eq 4 yields the following form for the proton inventory,

$$\frac{i_n}{i_0} = \frac{k_n}{k_0} = \frac{(1+2r)(1-a_1n)(1-a_2n)}{(1-a_1n)+2r(1-a_2n)} \quad (6)$$

where r is the ratio of the rate constants for the two distinct processes of Figure 4 (lower) in H₂O buffer; H₂ production is rate-limiting for r small, electron/proton transfer is rate-limiting for large r . Inspection of eq 6 shows that the limiting cases are given by eq 7,

$$r = \frac{k_2^o}{k_1^o} \begin{cases} \rightarrow 0; H_2 \text{ Rate Limiting:} & \frac{i_n}{i_0} = (1 - a_2n) \\ \rightarrow \infty; ET \text{ Rate Limiting:} & \frac{i_n}{i_0} = (1 - a_1n) \end{cases} \quad (7)$$

To demonstrate the overall behavior of the proton inventory (eq 6) for H₂ production as a function of r and n , Figure 5 plots i_n/i_0 (eq 6) as a function of these variables for a scenario in which H₂ formation has an isotope effect, KIE₂ = 2.7 as seen experimentally, but [e⁻/H⁺] delivery is rate-limited by transfer of the electron to MoFe protein, and thus KIE₁ = 1. Such assumed behavior for ET parallels our finding that there is no solvent kinetic isotope effect (KIE = 1) during electron transfer to MoFe protein from the physiological Fe protein electron donor,²⁵ and is returned to shortly. As $r \rightarrow 0$, H₂ production becomes rate limiting; the inventory becomes roughly linear for $r \lesssim 1/10$, asymptotically becoming a straight line with KIE₂ with further decrease in r , as shown in eq 7. Conversely, as r increases above ~0.1–0.2, the apparent KIE at $n=1$ decreases and the proton inventory bows upward, most extremely at $r \sim 1$; such behavior in an experiment might well suggest involvement of multiple protons, but in the present scenario it is due to the interplay between the individual kinetic steps of Figure 4. With further increase in r , electron transfer becomes rate limiting and the KIE $\rightarrow 1$, as assumed.

The experimental behavior is well described by the model of eq 6, Figure 5. Thus, the linear proton inventory predicted by the model for $r < 1/10$ and the chosen KIE_i matches well with experiment at high [CC] = 667 μM (Figure 2), indicating that in these experiments a single proton is coupled to the rate-limiting H₂ release. As presented in Figure 5, when [CC] is decreased by over ten-fold, to 50 μM, with the corresponding decrease in the ET rate constant, k_1^o , the system falls away from the $r \rightarrow 0$ limit with its linear proton inventory (Figure 2) and the proton inventory curve bows upward with a decrease in the KIE observed at $n = 1$. Figure 5 shows that the inventory at 50 μM CC is well captured by eq 6 with the assumed KIE_i and a ratio, $r \sim 0.5$. The latter value in turn implies that the faster electron transfer at 667 μM CC corresponds to a ratio, $r \sim 0.04$, which is well into the limiting $r \rightarrow 0$ behavior of a linear proton inventory (Figure 5), as observed experimentally (Figure 2). We further note that plots of eq 6 as a function of the variables, [KIE₁, r], show that the shape of the proton inventory and value of the apparent KIE at $n = 1$ as measured for [CC] = 50 μM

(Figure 5) in fact require that $KIE_1 \sim 1$ (≈ 1.2), consistent with the limiting assumption $KIE_1 = 1$ used in constructing Figure 5.

These observations provide a clear demonstration of the validity of the kinetic model of Figure 4 (lower) with the parameters utilized in Figure 5 for application to the bioelectrocatalysis data reported here. Most importantly, however, as noted above, the extended scheme involving H_2 formation at $E_4(4H)$ (Figure 4 (top)) behaves identically.

Non-Exchangeable Proton

A bridging H^-/D^- of $E_2(2H)$ or $E_4(4H)$ generated during turnover in an isotopically mixed solvent is of course derived from solvent, but it does not exchange with solvent on turnover timescales, as shown long ago by Burgess and coworkers, and recently confirmed by us.^{7,26} Thus, for rate-limiting H_2 formation ($r \rightarrow 0$), if the bridging H^-/D^- is involved in the rate-limiting process, rather than the H^+ bound to S, then in an isotopically mixed solvent the steady-state current will be the sum of the currents for the independent reactions of the H^- and D^- forms:

$$i_n = (1 - f_n)i_0 + f_n \frac{i_0}{KIE_2}; \quad f_n = p \cdot n \quad (8)$$

where f_n is the fraction of $E_2(2H)$ or $E_4(4H)$ with a bridging deuteride and the constant, p , is the equilibrium partition coefficient that relates the ratio of the D and H populations of the bridge (f_n) relative to the ratio in the mixed-isotope buffer (n). This equation is appropriate as long as the number of deuterons in the solvent is much greater than the amount of MoFe protein. Given the concentration of hydrons in water is ~ 110 M, this obviously holds for any possible experiment in an H_2O/D_2O mixture. Equation 8 is straightforwardly rewritten as,

$$\frac{i_n}{i_0} = (1 - a'_2 n); \quad a'_2 = p \cdot a_2 \quad (9)$$

which is identical in form to that for an exchangeable proton, eq 5. In the general case, where the system is not fully in the limit of rate-limiting H_2 formation, the general eq 5 again applies, with only the simple substitution of a'_2 for a_2 . In short, when a single hydron is involved in the rate-limiting production of H_2 , the proton inventory associated with current during turnover is linear regardless of whether or not the hydrogen exchanges rapidly with solvent; only the meaning of the calculated KIE is altered, eqs 5, 9. We note that to the best of our knowledge, this issue has not been addressed previously.

The experimental measurements reported here, as analyzed with this kinetic treatment of the proton inventory, leads to the following conclusions: (i) the formation of H_2 is rate limiting in electrocatalytic production of H_2 by electrode-bound MoFe protein, and as a result the measured KIE corresponds to this process, $KIE_2 = 2.7$ at 298 K, while the variation of the inventory with $[CC]$ confirms that $KIE_1 \sim 1$; (ii) formation of the transition state for H_2 formation involves motion of a single hydron. However, (iii) the analysis leading to eqs 8, 9

shows that the measurements do not differentiate between involvement of the bridging H^-/D^- , which is not solvent-exchangeable, or of the H^+/D^+ on sulfur, which is. Calculations presented below resolve this uncertainty. Finally, comparison of this process at ambient temperature with the previous measurement for relaxation of $\text{E}_2(2\text{H})$ with H_2 release in frozen solution shows a slight increase in the KIE with cooling: from $\text{KIE}_{\text{E}_2} = 2.7$ at ambient to $\text{KIE}_{\text{E}_2} \sim 3$ in frozen solid at 243 K.²⁷

Altering the rate limiting step

We previously showed that substitution of key amino acids in the MoFe protein that surround the active site FeMo-cofactor (residue positions relative to FeMo-cofactor shown in Figure S2) can alter substrate reduction chemistry. Here, we have analyzed several MoFe proteins with key amino acid substitutions by the electrochemical method to probe their role in the rate limiting step of H_2 formation (voltammograms shown in Figures S3–S6). Proton inventories were generated for wild type MoFe protein, $\alpha\text{-70}^{\text{Val}\rightarrow\text{Ile}}$ MoFe protein, $\alpha\text{-70}^{\text{Val}\rightarrow\text{Ala}}/\alpha\text{-195}^{\text{His}\rightarrow\text{Gln}}$ MoFe protein, $\beta\text{-98}^{\text{Tyr}\rightarrow\text{His}}$ MoFe protein, and nifX-FeMo-cofactor (Figure 6). For the latter sample, FeMo-cofactor is extracted from MoFe protein into the organic solvent N-methylformamide and then bound to purified carrier protein nifX. The resulting complex contains FeMo-cofactor in an environment different from FeMo-cofactor bound in the MoFe protein.¹⁸ As can be seen from the smaller slopes and difference in the endpoint ($n = 1$) of these plots compared to that for wild-type enzyme, all of the altered MoFe proteins and nifX-FeMo-cofactor show smaller KIE (eq 1). Although the magnitude of KIE was lowered by the substitutions, the observation of a linear proton inventory for all proteins demonstrates that the rate-limiting step has not changed and that a single hydron is involved. The differences in KIE induced by the substitutions could be explained by differences in reactivity of the metal hydrides in these proteins, or a difference in the bonding/acidity of the proton bound to sulfide.

Atomistic Interpretation of the Kinetic Isotope Effect and Proton Inventory

Previous computational studies on a simplified model of nitrogenase, which included FeMo-cofactor and its ligands, revealed that the $\text{E}_2(2\text{H})$ state is characterized by a hydride, asymmetrically bridging $\text{Fe}_2\text{-Fe}_3$ and a proton on a nearby $\mu_2\text{-S}$ atom (Figure 7),²³ and we examine H_2 production by this state as representative of hydride protonations on FeMo-cofactor. This state easily releases H_2 ($G^\ddagger = +29.4$ kJ/mol) restoring E_0 . A more exhaustive computational analysis of the mechanism of H_2 release, carried out in the present work, provided an estimated $\text{KIE} = 3.2$ at 298 K, in excellent agreement with the experimentally measured $\text{KIE} = 2.7$.

The calculations provide an atomic level understanding of the single-hydron proton inventory measurement by indicating that only the proton (S-H) moves appreciably as the system evolves from $\text{E}_2(2\text{H})$ to the transition state $\text{E}_2(2\text{H})^\ddagger$, as shown in two animations included in the SI (animations S1 and S2). Specifically, the calculations show that the formation of H_2 results from the protonation of the hydride, whereby the S-H bond breaks heterolytically with concomitant movement of the proton toward the bridging hydride. As shown in Figure 7, at the transition state, $\text{E}_2(2\text{H})^\ddagger$, the $\text{H}\dots\text{H}$ moiety has already started

forming (H...H distance of 0.97 Å) and the S-H is fully broken, while the hydride remains tightly bound to one Fe atom.

The KIE is computed to result from the higher free energy barrier for the formation of D₂ relative to the formation of H₂ (32.3 kJ/mol and 29.4 kJ/mol, respectively). Decomposition of the free energy into its various contributions indicates that the difference in isotopic activation barriers is mostly a consequence of a change in the nuclear zero-point energy of the S-H/D bond in the reactant E₂(2H) state (Figure 7, bottom). Upon isotopic substitution, the free energy of both E₂(2H) and the transition state E₂(2H)[‡] decrease because of the smaller vibrational zero-point energy contribution. However, the decrease is larger for E₂(2H) (both S-D and Fe-D bonds) than for E₂(2H)[‡] (only Fe-D bond). In short, the main contribution to the KIE is the loss of the S-D/H bond in the transition state.

Conclusions

Mediated electrochemistry with electrode-confined nitrogenase MoFe protein eliminates the need for the delivery of electrons from the Fe protein, with the associated hydrolysis of ATP. This bypasses the rate limiting Fe protein cycle during turnover, revealing the rate-limiting step in substrate reduction at the FeMo-cofactor active site. The rate-limiting step of H₂ formation when nitrogenase is acting as a 'hydrogenase' is not associated with electron/proton delivery, but rather is associated with hydride protonation. Exploration of the effect of H vs. D isotopes on the formation of H₂ in this electrochemical system indicated that the rate-limiting step involves a single H atom. DFT calculations reveal that formation of the transition state E₂(2H)* involves the breaking of the S-H bond, with the proton attacking the hydride (Fe-H-Fe) to form H₂. The activation barrier for such proton transfer is modulated by the environment around the FeMo-cofactor, and hence altering the amino acids around the FeMo-cofactor would be predicted to have a pronounced effect in partition of electrons during reduction of other substrates. To our knowledge, this study is the first to use such an approach to reveal the mechanism for H₂ formation by an enzyme, thus providing both insights into the reactivity of hydrides at the nitrogenase active site, and an example that can be followed for other enzymes and even biomimetic complexes and inorganic systems in general.

Supplementary Material

Refer to Web version on PubMed Central for supplementary material.

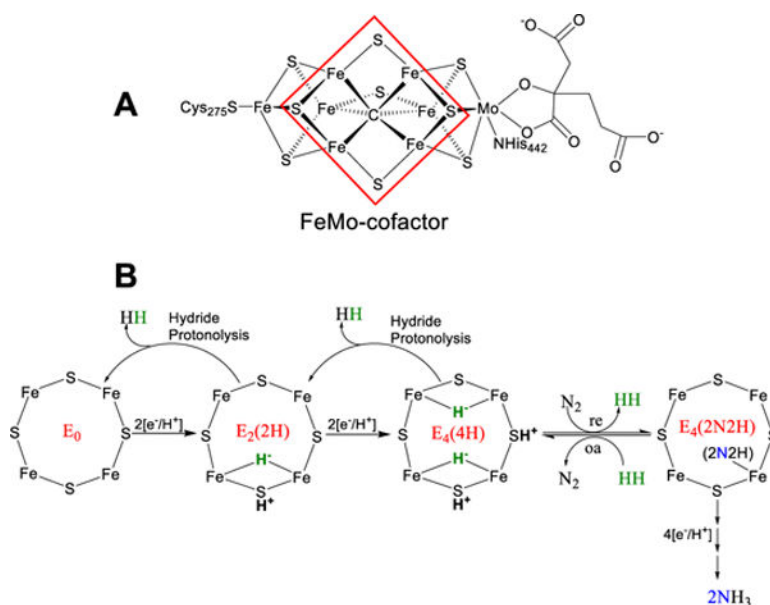
Acknowledgments

Work by LCS and DRD was supported by the U.S. Department of Energy (DOE), Office of Science, Basic Energy Sciences (BES) under award numbers DE-SC0010687 and DE-SC0010834. Work by SR was also supported by the DOE, Office of Science, BES, Chemical Sciences, Geosciences, and Biosciences Division under separate contract. Work by BMH was supported by the National Institutes of Health under award GM 111097.

References

1. Smil, V. Enriching the earth: Fritz Haber, Carl Bosch, and the transformation of world food production. MIT Press; Cambridge, Mass: 2001.

2. Yang Z-Y, Khadka N, Lukoyanov D, Hoffman BM, Dean DR, Seefeldt LC. Proc Natl Acad Sci USA. 2013; 110:16327. [PubMed: 24062454]
3. Hoffman BM, Lukoyanov D, Yang Z-Y, Dean DR, Seefeldt LC. Chem Rev. 2014; 114:4041. [PubMed: 24467365]
4. Lukoyanov D, Yang Z-Y, Khadka N, Dean DR, Seefeldt LC, Hoffman BM. J Am Chem Soc. 2015; 137:3610. [PubMed: 25741750]
5. Lukoyanov D, Khadka N, Dean DR, Raugei S, Seefeldt LC, Hoffman BM. Inorg Chem. 2017; 56:2233. [PubMed: 28177622]
6. Lukoyanov D, Khadka N, Yang Z-Y, Dean DR, Seefeldt LC, Hoffman BM. J Am Chem Soc. 2016; 138:1320. [PubMed: 26788586]
7. Lukoyanov D, Khadka N, Yang Z-Y, Dean DR, Seefeldt LC, Hoffman BM. J Am Chem Soc. 2016; 138:10674. [PubMed: 27529724]
8. Hoffman BM, Lukoyanov D, Dean DR, Seefeldt LC. Acc Chem Res. 2013; 46:587. [PubMed: 23289741]
9. Thorneley, RNF., Lowe, DJ. Molybdenum Enzymes. Spiro, TG., editor. Vol. 7. Metal Ions in Biology; Wiley-Interscience Publications; New York: 1985. p. 221-284.
10. Igarashi RY, Laryukhin M, Dos Santos PC, Lee H-I, Dean DR, Seefeldt LC, Hoffman BM. J Am Chem Soc. 2005; 127:6231. [PubMed: 15853328]
11. Lukoyanov D, Yang Z-Y, Dean DR, Seefeldt LC, Hoffman BM. J Am Chem Soc. 2010; 132:2526. [PubMed: 20121157]
12. Hageman RV, Burris RH. Proc Natl Acad Sci US A. 1978; 75:2699.
13. Seefeldt LC, Hoffman BM, Dean DR. Annu Rev Biochem. 2009; 78:701. [PubMed: 19489731]
14. Thorneley RNF, Lowe DJ. Biochem J. 1983; 215:393. [PubMed: 6316927]
15. Yang Z-Y, Ledbetter R, Shaw S, Pence N, Tokmina-Lukaszewska M, Eilers B, Guo Q, Pokhrel N, Cash VL, Dean DR, Antony E, Bothner B, Peters JW, Seefeldt LC. Biochemistry. 2016; 55:3625. [PubMed: 27295169]
16. Milton RD, Abdellaoui S, Khadka N, Dean DR, Leech D, Seefeldt LC, Minteer SD. Energy Environ Sci. 2016; 9:2550.
17. Christiansen J, Goodwin PJ, Lanzilotta WN, Seefeldt LC, Dean DR. Biochemistry. 1998; 37:12611. [PubMed: 9730834]
18. Lukoyanov D, Pelmeshnikov V, Maeser N, Laryukhin M, Yang TC, Noodleman L, Dean DR, Case DA, Seefeldt LC, Hoffman BM. Inorg Chem. 2007; 46:11437. [PubMed: 18027933]
19. Kohen, A., Limbach, HH. Isotope effects in chemistry and biology. Taylor & Francis; Boca Raton: 2006.
20. Becke AD. Phys Rev A. 1988; 38:3098.
21. Perdew JP. Phys Rev B. 1986; 33:8822.
22. Klamt A, Schüürmann G. J Chem Soc, Perkin Trans. 1993; 2:799.
23. Khadka N, Dean DR, Smith D, Hoffman BM, Raugei S, Seefeldt LC. Inorg Chem. 2016; 55:8321. [PubMed: 27500789]
24. Valiev M, Bylaska EJ, Govind N, Kowalski K, Straatsma TP, Van Dam HJJ, Wang D, Nieplocha J, Apra E, Windus TL, de Jong WA. Comput Phys Commun. 2010; 181:1477.
25. Mayweather D, Danyal K, Dean DR, Seefeldt LC, Hoffman BM. Biochemistry. 2012; 51:8391. [PubMed: 23050654]
26. Burgess BK, Lowe DJ. Chem Rev. 1996; 96:2983. [PubMed: 11848849]
27. Lukoyanov D, Yang Z-Y, Duval S, Danyal K, Dean DR, Seefeldt LC, Hoffman BM. Inorg Chem. 2014; 53:3688. [PubMed: 24635454]

**Figure 1.**

(A) Schematic representation of the FeMo-cofactor with α -Cys²⁷⁵, α -His⁴⁴² and *R*-homocitrate as ligands. The red highlighted square represents the catalytically active 4Fe-4S face of the FeMo-cofactor. (B) Shown are the E_n states of FeMo-cofactor during accumulation of the first four electrons/protons, along with the reductive elimination/oxidative addition (*re/oa*) mechanism at $E_4(4H)$. The “2N₂H” intermediate implies a species at the diazene reduction level of unknown structure and coordination geometry.

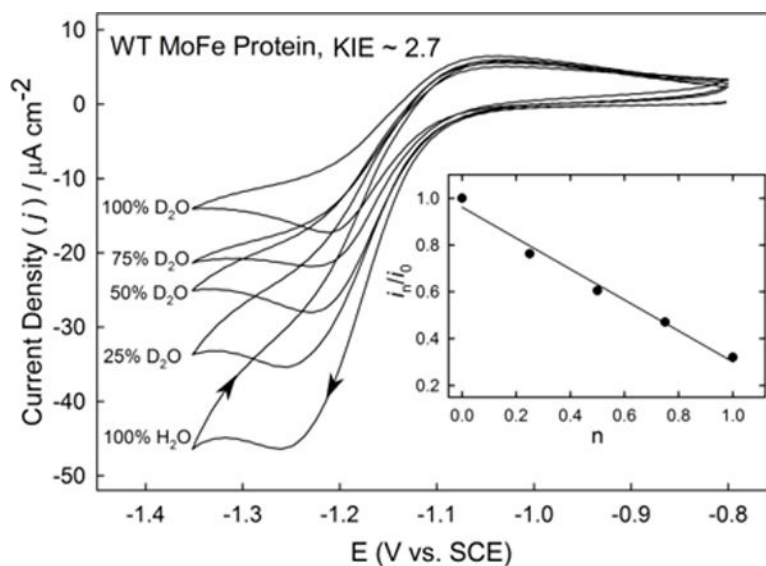


Figure 2.

Cyclic voltammogram (CV) for wild type MoFe protein. CV for wild type MoFe protein was collected using CC as an electron mediator. Shown is the current density (j) as a function of the applied potential at different percentages of D_2O . The current was measured at -1.26 V, -1.25 V, -1.24 , -1.24 V, and -1.24 V for 100% H_2O , 25% D_2O , 50% D_2O , 75% D_2O and 100% D_2O , respectively. The non-catalytic current was subtracted from the observed current to get the net catalytic current. In the inset, the ratio of net current at n fraction of D_2O (i_n) to the catalytic current in 0 % D_2O (i_0) is plotted against the mole fraction (n) of D_2O . The line is a fit of the data to the Gross-Butler equation for a one proton transfer (eqn 1), where the solvent isotope effect is 2.7. Condition: 250 mM HEPES pH/pD = 7.2), 667 μ M CC and a scan rate of 2 mV/s at 23°C.

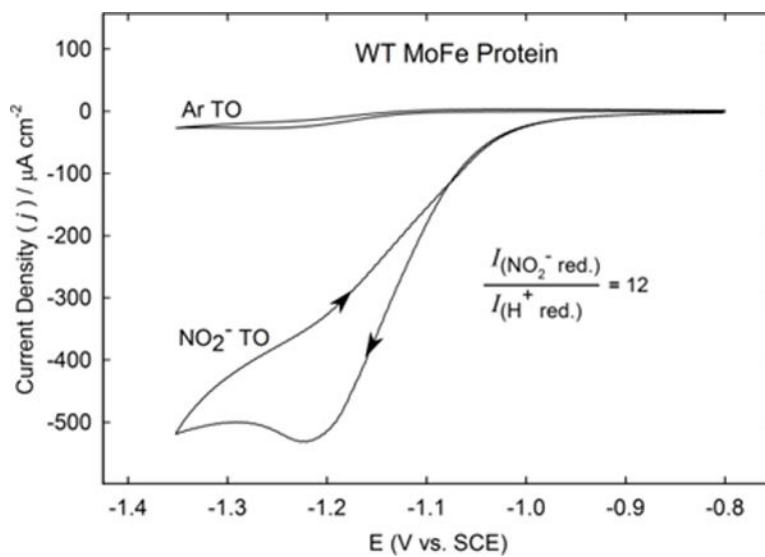


Figure 3. Cyclic voltammogram for wild type MoFe protein turnover (TO) under Ar (Ar TO) and turnover in nitrite (NO_2^- TO). Condition: 250 mM HEPES pH 7.2, 667 μM CC, 50 mM NO_2^- and scan rate of 2 mV/s at 23°C.

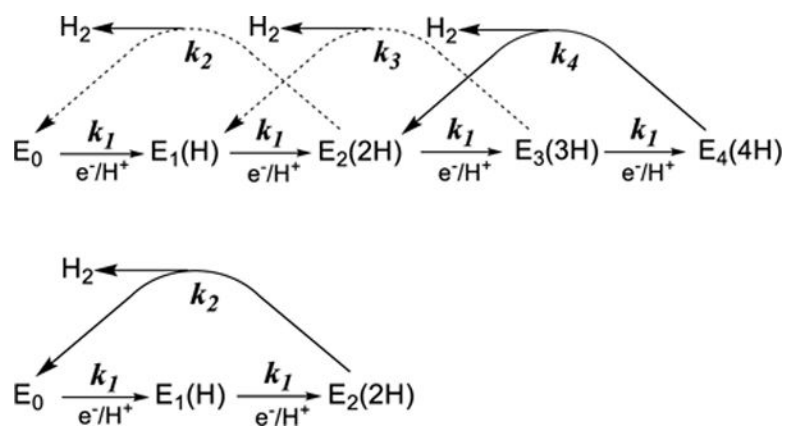


Figure 4. (Top) Kinetic scheme for accumulation of protons and electrons on FeMo-co and loss of H₂. The rate constants for ET are all taken to be k_1 , while the rate constants for H₂ loss are k_2 , k_3 , and k_4 . (Top) Shown is relaxation from E₄(4H) (solid line), E₃(3H) and E₂(2H); dashed lines indicate pathways suppressed in mediated electrochemistry (see text). (Bottom) Equivalent truncated catalytic cycle for H₂ formation involving E₀, E₁, and E₂.

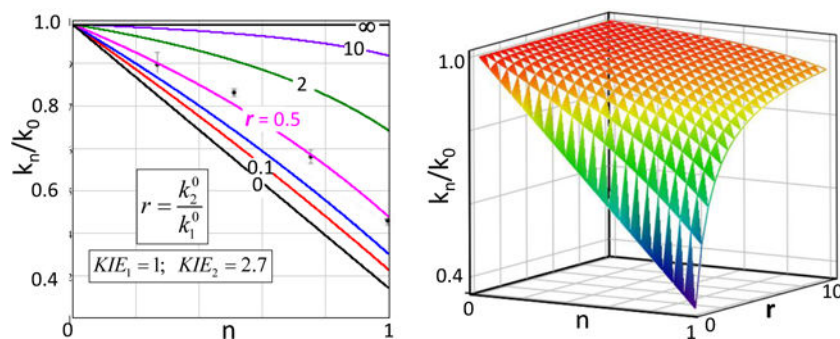


Figure 5. Proton inventory plots (eq 6). **(Left)** Predicted plots of i_n/i_0 versus fraction of D_2O in buffer (n) at the indicated KIE_i for selected values of r ; also, blue, 0.2; points, inventory as measured for $[CC] = 50 \mu M$ **(Right)** A 3D plot of the proton inventory (eq 6) as function of (n, r).

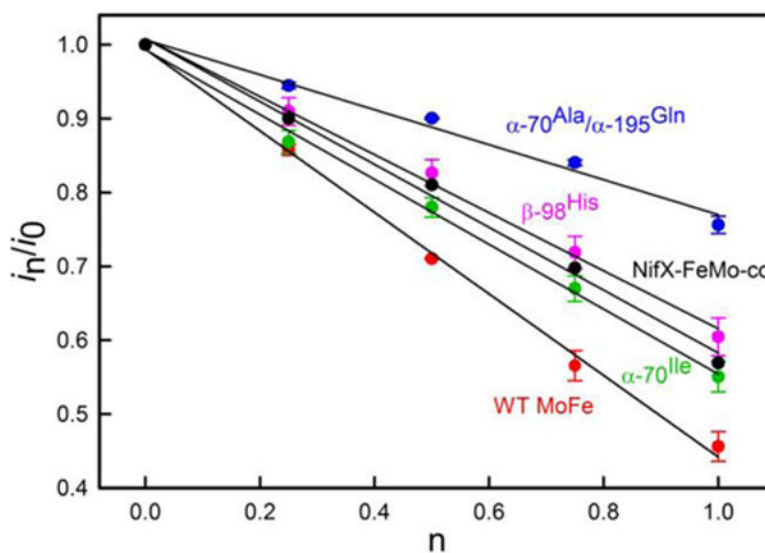


Figure 6. Proton inventory plot MoFe proteins. Shown are the proton inventory plots for wild type (red), β -98^{Tyr} \rightarrow ^{His} (magenta), α -70^{Val} \rightarrow ^{Ile} (green), α -70^{Val} \rightarrow ^{Ala}/ α -195^{His} \rightarrow ^{Gln} (blue) MoFe protein and nifX-FeMo-cofactor (black). Condition: 250 mM HEPES pH or pD 7.2, 667 μ M CC, and scan rate of 2 mV/s at 23°C.

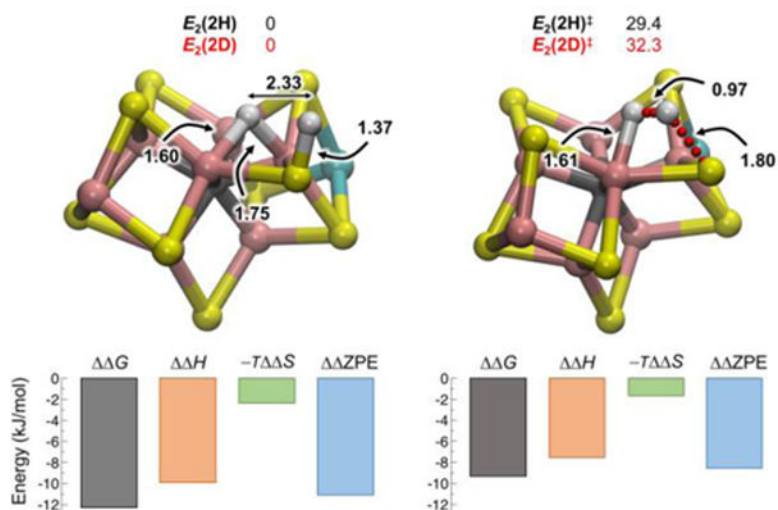


Figure 7. Structure of the E₂(2H) state and the transition state E₂(2H)[‡] for the release of H₂ (upper panels; for clarity, only the FeMo-co core is shown). Relevant distances are reported in Å along with the free energy of E₂(2H)[‡] and E₂(2D)[‡] relative to E₂(2H) and E₂(2D), respectively. The lower panels report the free energy G of E₂(2D) and E₂(2D)[‡] relative to E₂(2H) and E₂(2H)[‡] along with the enthalpic (H), entropic ($-T S$) and nuclear zero point energy (ZPE) contributions to G . All energies in kJ/mol.